Comprehensive Assessment of Urban Greening and Environmental Quality Based on Multi-Source Data Fusion: A Case Study of Hitachi City

Dongmin Yin[1] and Terumitsu Hirata[2,*]

[1]Department of Urban and Civil Engineering, Graduate School of Science and Engineering, Ibaraki University, Hitachi, Japan
[2]Department of Urban and Civil Engineering, Faculty of Applied Science and Engineering, Ibaraki University, Hitachi, Japan
*Corresponding author
Email: 22nd313y@vc.ibaraki.ac.jp (D.Y.); terumitsu.hirata.a@vc.ibaraki.ac.jp (T.H.)
Manuscript received December 10, 2024; revised March 19, 2025; accepted March 31, 2025; published August 5, 2025

***Abstract*—As urbanization accelerates, environmental challenges such as air pollution, noise, urban heat islands, and biodiversity loss have intensified. Urban greening is widely recognized as a key strategy for improving environmental quality. This study introduces the Urban Greening Environmental Quality Index (UGEQI), a multi-source data fusion model integrating the Green View Index (GVI), Normalized Difference Vegetation Index (NDVI), Air Quality Index (AQI), Land Surface Temperature (LST), and noise pollution. Applied to Hitachi City, Japan, results show an average GVI of 22.40%, below the 25% satisfaction threshold, with notable differences across road types (e.g., highways: 25%, residential roads: 17.6%). NDVI exhibits substantial seasonal variation, peaking at 0.31 in summer and dropping to 0.18 in winter. The UGEQI model assigns weights using the entropy method: NDVI (24.7%), GVI (24.6%), LST (19.2%), noise (16.9%), and AQI (14.5%). Regression analysis (R^2 = 0.690) confirms a strong correlation between GVI and NDVI, highlighting their interdependence. These findings emphasize the need for targeted greening strategies, particularly in dense urban areas. The UGEQI model serves as a replicable framework for cities facing similar environmental challenges, aiding in developing more effective urban greening strategies to enhance environmental quality and residents' well-being.**

***Keywords*—urban greening, environmental quality, multi-source data fusion, green view index, NDVI, UGEQI**

I. Introduction

A. Research Background

With the accelerated pace of urbanization, cities around the globe are grappling with a series of serious environmental issues, including air pollution [1], noise pollution [2], the urban heat island effect, and a decline in biodiversity [3, 4]. These challenges not only jeopardize the health of ecosystems but also profoundly affect the quality of life and mental well-being of urban residents [5]. Consequently, the effective enhancement of urban environmental quality has emerged as a critical concern in urban planning and environmental management.

Urban greening is widely recognized as an effective ecological intervention in this context. Research indicates that urban greening can significantly improve air quality, reduce urban temperatures, decrease carbon dioxide emissions, mitigate flooding [6–8], enhance urban water resources [9] and promote biodiversity [10, 11]. Additionally, it contributes to reducing environmental air pollution and noise, thereby improving overall quality of life [12, 13]. Furthermore, urban greening also yields multiple positive social effects, such as enhancing well-being [14, 15], reducing the incidence of violence [16], and increasing feelings of social safety [17, 18].

However, traditional methods for assessing urban greening often rely on singular metrics, such as the NDVI [19], per capita green space area [20], green space volumetric ratio [21], forest cover [22], and vegetation diversity index [23]. These studies predominantly focus on the quantitative analysis of urban green spaces' quantity, quality, and value, which may fail to comprehensively reflect citizens' actual perceptions and the multifaceted impacts of greening on the environment. The GVI has gained scholarly attention as an emerging metric for evaluating urban greening in recent years. Defined as the percentage of green vegetation in street view images or images of specific locations [24], GVI not only reflects public perceptions and satisfaction regarding greening through visual assessments but also highlights the significant influence of large trees and their distribution on urban greening. Furthermore, it effectively characterizes the visual greening along roadways, providing crucial insights for the planning and managing urban green spaces [25, 26]. Therefore, integrating GVI with traditional metrics such as NDVI for a comprehensive assessment aids urban planners in making more informed decisions [27].

In assessing environmental quality, the AQI and LST are commonly employed indicators [28, 29]. Research demonstrates that urban greening is vital in enhancing air quality, particularly in significantly reducing concentrations of pollutants such as PM2.5, sulfur dioxide, and nitrogen monoxide [30, 31]. Additionally, greening contributes to lower urban temperatures through evapotranspiration and shading effects, alleviating the urban heat island phenomenon [32]. Regarding noise pollution, greening can mitigate the impact of traffic noise on residents by acting as a barrier and absorbing sound [33].

Despite existing studies elucidating the multifaceted benefits of urban greening for environmental quality, most assessment methods remain focused on unidimensional analyses, lacking a holistic evaluation of the comprehensive benefits of urban greening. Thus, introducing a multidimensional data-based urban environmental quality assessment model, such as the UGEQI, aims to address this gap. By considering multiple dimensions, including GVI, NDVI, LST, AQI, and noise pollution index, the UGEQI model can provide a more scientifically sound and comprehensive basis for formulating urban greening strategies.

B. Research Objectives

This study aims to develop a comprehensive model for assessing urban greening and environmental quality through integrating multi-source data. Using Hitachi City as a case study, this research not only focuses on the visual benefits of urban greening, as measured by the GVI, but also incorporates various dimensions including vegetation health NDVI, AQI, LST, and noise pollution. This approach culminates in the UGEQI proposal. Through this model, the study explores the levels of greening across different road types in Hitachi City, the seasonal variations in greening, and their collective impact on environmental quality. The primary objectives of this research are as follows:

1) Analyze the spatiotemporal distribution of the Green View Index (GVI) to identify variations in urban greening across different road types and seasonal changes.

2) Investigate the coupling relationship between GVI and the Normalized Difference Vegetation Index (NDVI) to explore their temporal correlations and better understand the intrinsic link between visual greening and vegetation cover.

3) Develop the Urban Greening Environmental Quality Index (UGEQI) model using multi-source data fusion to evaluate the multidimensional impacts of urban greening, including visual enhancement, temperature regulation, air quality improvement, and noise mitigation.

4) Provide scientific guidance for urban planners and policymakers, facilitating the development of more precise and effective greening strategies to enhance urban environmental quality and improve residents' well-being.

C. Research Framework

This study follows a structured framework to ensure methodological rigor and scientific validity. First, it provides an overview of the study area—Hitachi City—and details the data acquisition, preprocessing, and analytical methods. Next, a spatiotemporal analysis of GVI is conducted to examine variations across road types and seasonal trends. Subsequently, the seasonal correlation between NDVI and GVI is explored to elucidate the coupling relationship between vegetation health and visual greening. The study then develops the UGEQI model, describing the selection of key indicators, computational methods, and entropy-based weight allocation. Based on the model's findings, the spatiotemporal variations in greening levels and environmental quality in Hitachi City are analyzed. Finally, policy recommendations are proposed based on the research results, followed by a discussion on the study's limitations and potential future research directions, contributing to a deeper understanding of sustainable urban greening strategies.

II. Study Area and Data

A. Study Area

This study focuses on Hitachi City, located in the northern part of Ibaraki Prefecture, Japan, as shown in the Fig. 1. Situated along the Pacific coast, Hitachi City experiences a temperate oceanic climate with distinct seasonal variations. The spring and summer months are characterized by moderate temperatures and abundant rainfall, fostering vigorous vegetation growth. In contrast, the autumn and winter seasons are marked by drier conditions and lower temperatures, leading to a gradual decline in vegetation activity. These seasonal fluctuations significantly impact urban air quality, temperature regulation, and vegetation coverage, particularly regarding improved air quality during the summer and a reduction in the urban heat island effect during the winter.

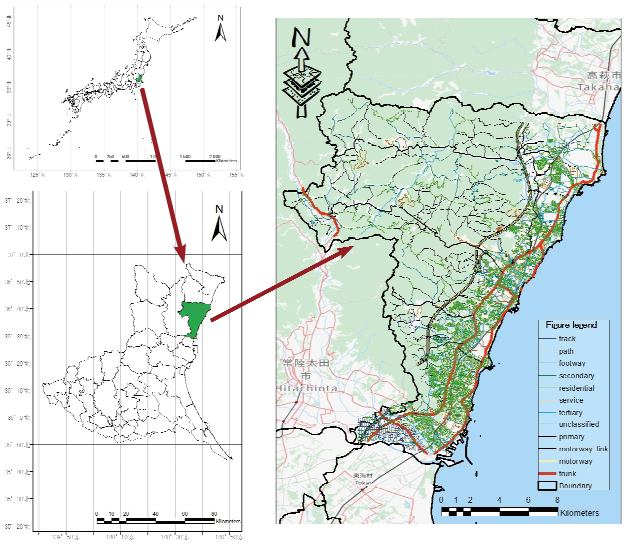

Fig. 1. Location map of the study area.

Covering a total area of 225.73 km^2, Hitachi City has an urbanized region spanning 50.61 square kilometers and a resident population of approximately 170,000. Since 1985, the population has gradually decreased due to declining birth rates and industrial restructuring. Nevertheless, the city boasts a highly developed transportation network, featuring a total road length of 1,697.5 km, including 23.7 km of expressways, 55.8 km of national roads, 77 km of prefectural roads, and 1,539 km of municipal streets. The city's transportation infrastructure is well-equipped, with the Joban Expressway traversing the area and accommodating substantial traffic flow, thus facilitating the use of traffic volume data as a proxy for noise in this study.

Regarding urban greenery, Hitachi City is endowed with rich vegetative resources and a comprehensive park system, comprising 261 parks, including 241 small neighborhood parks and 20 medium to large parks. Approximately 4,148 tall trees and 162,353 low shrubs are planted along urban roadways, highlighting these green resources' significant role in regulating urban environmental quality. Through a comprehensive analysis of indicators such as the GVI and the NDVI, a holistic assessment of the city's greening levels can be achieved from both visual and ecological perspectives.

As an ideal case for the UGEQI study, Hitachi City presents typical conditions for integrating multidimensional environmental factors. The city's unique characteristics are evident in the interplay of greening strategies, climatic conditions, traffic volumes, and environmental quality. By combining multiple indicators, including GVI, NDVI, LST, AQI, and noise index, this study provides a comprehensive and nuanced perspective for assessing urban green environment quality. This offers scientific guidance for urban planning in Hitachi City and serves as a valuable reference for similar research and strategic development in other cities facing comparable environmental contexts.

B. Data Sources

1) GVI

The acquisition of data for the GVI consists of two components: first, the collection of street latitude and longitude data, followed by gathering streetscape images. For the street coordinates, the author initially sourced the road network data for Hitachi City from OpenStreetMap, subsequently employing equidistant sampling within ArcGIS. Concerning the sampling distance for streetscapes, researchers have traditionally employed equidistant measurements along the road, establishing various interval standards for greenery calculations based on distinct research objectives and environmental characteristics, including distances of 20m [34], 50m [35], 100m [36], and 200m [37]. As shown in Fig. 2, this study opts to extract point data from the road network layer at intervals of 20 m, ultimately obtaining the latitude and longitude coordinates for the point data according to different road types.

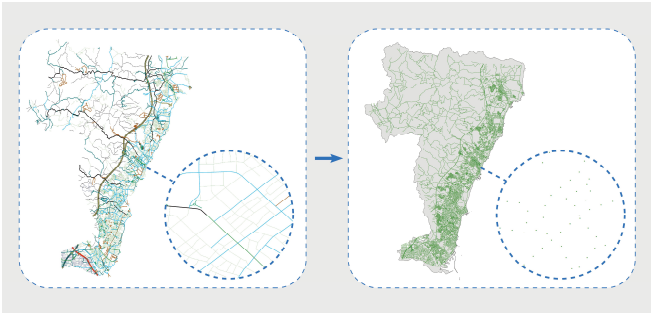

Fig. 2. Schematic representation of the conversion of line data to point features.

Regarding street view data collection, there are primarily two methods for acquiring GVI images: one involves manual collection on-site [38], while the other utilizes street view maps [39]. Manual collection typically requires the camera to be fixed at a height of approximately 1.6m, corresponding to adult eye level. It employs a 22mm lens that closely mimics the visual perspective of the human eye. In contrast, street view images can be obtained through API interfaces provided by platforms such as Baidu, Google, and Tencent, allowing for the download and retrieval of static street view imagery [40–42]. This method significantly simplifies the workforce, resources, and time required for manual surveys.

Fig. 3. Schematic representation of the stitching process for street view acquisition.

For this study, the Google Street View API was selected as the platform for data acquisition. Utilizing the obtained geographical coordinates, code was written to collect corresponding static images of the streets systematically. Each location yielded three images from distinct angles, with a horizontal field of view set at 120° and a vertical field at 60°, slightly exceeding the comfortable rotational range of the human eye (55°) to ensure the closest approximation to human visual perception. The following Fig. 3 is a schematic diagram of a panoramic image after stitching three street view images.

After data cleaning, 62,410 coordinate points were collected, corresponding to 187,230 street view images.

2) NDVI

The NDVI data, obtained through remote sensing technology, effectively reflects the extent of vegetation cover and its health status. This data is integrated with the GVI for comprehensive analysis. In this study, Sentinel-2 satellite data were utilized [43], comprising 33 sets of NDVI measurements collected from August 2020 to August 2023. The data acquisition was evenly distributed across different seasons, with all data points characterized by a cloud cover of less than 20%. The Sentinel-2 Level-2A satellite data has undergone radiometric, geometric, and atmospheric corrections, so NDVI calculations can be performed directly.

3) AQI

The AQI serves as a critical metric for quantifying and assessing levels of air pollution. The AQI is calculated based on the concentrations of several prevalent atmospheric pollutants. It effectively communicates air quality information to the public through concise numerical values and color-coded indicators, thereby aiding individuals in understanding the concentration of pollutant contaminants in the air and their potential health impacts. For this study, the air quality data were sourced from the atmospheric monitoring station 44 of the Hitachi City government in Ibaraki Prefecture [44]. 36 monthly average data points were collected from April 2020 to March 2023, encompassing six pollutants: sulfur dioxide, nitrogen dioxide, carbon monoxide, photochemical oxidants, suspended particulate matter, and PM2.5.

4) LST

Temperature data serves as a reflection of variations in LST, where regions exhibiting elevated surface temperatures often correlate with lower levels of urban greening. Monthly average temperature data can be utilized to assess the regulatory effects of greening on the urban thermal environment [45]. In this study, NASA's MODIS (Moderate Resolution Imaging Spectroradiometer) LST data has been extracted using Google Earth Engine [46], encompassing 484 sets of temperature data collected over three years from August 2020 to July 2023.

5) Noise Index Data (Traffic Volume Data)

Research indicates that higher traffic volumes in urban areas typically correlate with elevated noise levels. In Japan, a 2022 study assessed automotive traffic noise, revealing that the noise intensity increases with the classification of urban roads. For instance, the highest rate of excess noise was found near highways, affecting approximately 18.4% of households [47]. Consequently, this study proposes utilizing traffic volume data as a proxy for noise levels. Specifically, traffic volume data from three entrances and exits of the Joban Expressway in Hitachi City will serve as the proxy variables. The corresponding noise level data will be computed by applying established conversion methods between traffic volume and noise levels. The data source comprises monthly statistical records for various vehicle types collected between April 2022 and March 2023 [48].

III. Methodology and Results

A. Proposal of the UGEQI

1) Concept of UGEQI

The Comprehensive UGEQI is a holistic metric developed by the author, grounded in the fusion of multi-source data to assess urban environmental quality. This study selects the NDVI, GVI, LST, AQI, and noise index as the core indicators of UGEQI, which collectively encompass the primary dimensions of urban greening's impact on environmental quality:

a) Visual Dimension: GVI represents the visible greenery ratio along streets, reflecting residents' perceptual experiences.

b) Environmental Dimension: NDVI measures vegetation health and coverage, indicating the actual benefits of greening.

c) Atmospheric Dimension: AQI is introduced to represent the effectiveness of greening in pollutant removal and air purification, highlighting its role in mitigating air pollution.

d) Temperature Regulation Dimension: Utilizing LST data, this metric assesses the contribution of urban greening in alleviating the urban heat island effect.

e) Noise Pollution Dimension: Noise data is incorporated to evaluate the role of greening in reducing urban noise pollution.

These five indicators comprehensively and directly measure the multifaceted impacts of urban greening on ecological and residential environments. By integrating this data, UGEQI enables decision-makers understand and enhance urban environmental quality, providing practical guidance for green city planning.

2) Formulation

effects. Higher standardized values signify better greening effects for positive indicators (such as NDVI and GVI); conversely, for negative indicators (such as LST, AQI, and noise index), higher standardized values indicate poorer environmental quality. To standardize directional consistency, these negative indicators must be inverted during computation. Thus, the UGEQI formula is proposed as follows:

$$UGEQI = \omega_1 \times GVI + \omega_2 \times NDVI + \omega_3 \times (1 - AQI) + \omega_4 \times (1 - LST) + \omega_5 \times (1 - Noise\,Index) \quad (1)$$

where ω is the weight for different indexes.

3) Weight allocation

In this study, the entropy method is employed for weight allocation to ensure that the influence of various indicators in the Comprehensive UGEQI is determined based on the objectivity of the data itself. The entropy method is an objective weight allocation technique grounded in information theory, centered on each indicator's variability (i.e., the degree of numerical dispersion) to ascertain its weight. The entropy value reflects the uncertainty of a given indicator within the sample; a higher entropy indicates lower variability and less information content, thereby suggesting a lower weight. Conversely, a lower entropy indicates greater variability and higher information content, warranting a larger weight.

Compared to subjective expert scoring methods, the entropy method relies solely on the data, effectively mitigating biases stemming from human intervention and subjective judgment. This approach ensures that weight allocation is more scientific and objective. By utilizing the entropy method, indicators with substantial information content receive higher weights, while those with minimal data variation are assigned lower weights, thus better reflecting the actual conditions. The entropy method effectively integrates multidimensional indicators, ensuring that the influence of each indicator is appropriately represented in the final composite index and preventing any single indicator from dominating the results.

B. Calculation and Analysis of GVI

1) Deep learning model

Deep learning algorithms for image classification, object detection, and semantic segmentation can enhance the accuracy of GVI calculation. Models utilized include PSPNet [49], SegNet [50], an improved fully convolutional network model [51], backpropagation neural networks [52], and DeepLab [53]. These models have demonstrated excellence in image segmentation and classification tasks. This study employs a deep learning software based on the MobileNet V3-Large neural network, developed by the National Institute for Land and Infrastructure Management of the Ministry of Land, Infrastructure, Transport and Tourism of Japan in 2022, to investigate the GVI in street view images [54]. The training dataset for this software was created using GVI survey photos provided by local Japanese governments, including regions such as Shinjuku, Koto, and Musashino in Tokyo. The dataset consists of 150 original images, capturing a diverse range of urban landscapes and vegetation coverage across different seasons and weather conditions. Diverse image data were used for training to improve the model's generalization and accuracy in real-world scenarios. Data augmentation techniques, including image scaling, parallel translation, rotation, and horizontal flipping, were applied, expanding the original 150 images to 5,000, thus enriching the data resources for model training.

2) GVI calculation

In this study, the average GVI for each point is calculated using the mean GVI of three images taken from different angles. Since each image has a resolution of 600 by 300 pixels, the calculation formula is as follows:

$$GVI = \frac{\sum Area_{g\_i}}{\sum Area_{t\_i}} \times 100\% = \frac{\sum GVI_i}{i} (i = 3) \quad (2)$$

where GVI is the Green View Index, $Area_{g\_i}$ indicates the green area in the i-th image, and $Area_{t\_i}$ denotes the total area in the i-th image.

3) GVI evaluation criteria

According to the survey conducted by the Ministry of Land, Infrastructure, Transport and Tourism of Japan, when the GVI exceeds 25%, people perceive a significant amount of green vegetation [55]. To evaluate the GVI of the entire city in more detail, this study, in conjunction with the Japanese Ministry of Land, Infrastructure, Transport and Tourism's survey report and the "Kyoto Prefecture Green Promotion Plan" [56], proposes the following GVI evaluation criteria:

a) 0–10%: Considered too low, requiring immediate enhancement of the environmental greening level.

b) 10–18%: Relatively low, necessitating robust greening efforts to improve the GVI.

c) 18–25%: Acceptable, with ongoing optimization while maintaining current greening levels.

d) Above 25%: Meets the standard, with efforts to protect greening achievements and maintain high GVI levels.

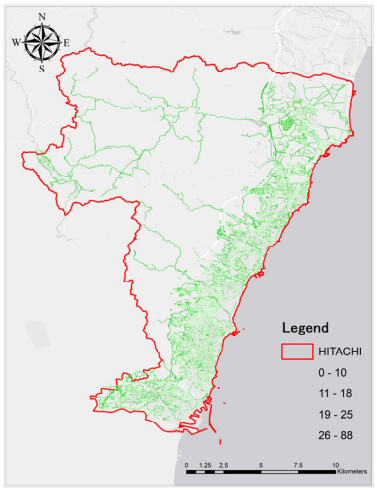

Fig. 4. GVI distribution nodes diagram.

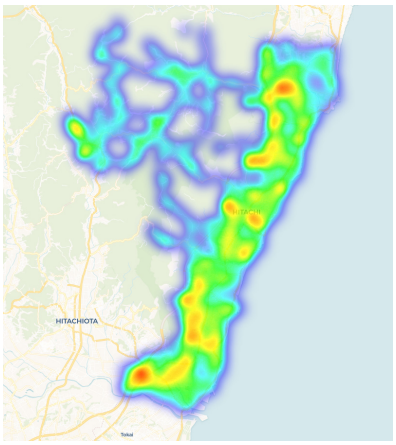

Fig. 5. Overall GVI hotspot map.

Based on this standard, the author conducts a comprehensive analysis of the distribution of the GVI. After calculating the GVI, the author integrates all ArcGIS datasets according to the classification criteria. The geographical coordinates serve as the framework, with the GVI as the focal point for visualization, resulting in a schematic representation of the GVI distribution nodes in Hitachi City, as illustrated in Fig. 4.

Fig. 5 presents the overall GVI hotspot map. It is evident from the illustration that the GVI exhibits a generally balanced distribution across the urban landscape, with specific areas displaying elevated GVI values, indicating the presence of substantial urban green spaces in their vicinity.

4) Overall GVI characteristics

Fundamental statistical analysis of the data reveals the average GVI and its variability for Hitachi City. As shown in Fig. 6, the average GVI is 22.40%, with a standard deviation of 18.29%, a variance of 334.59%, and a median of 17.32%. Overall, the average GVI exceeds 20%, indicating relatively good data, although it has not reached 25%. Therefore, there is room for optimization. The proportion of GVI within different ranges is as follows: 29% for 0–10%, 22.69% for 10–18%, 13.87% for 18–25%, and 34.44% for over 25%, with the highest proportion observed in the latter category. The overall distribution shows a sharp increase followed by a gradual decrease, peaking at a GVI of 9%. 66.56% of observation points have a GVI below 25%.

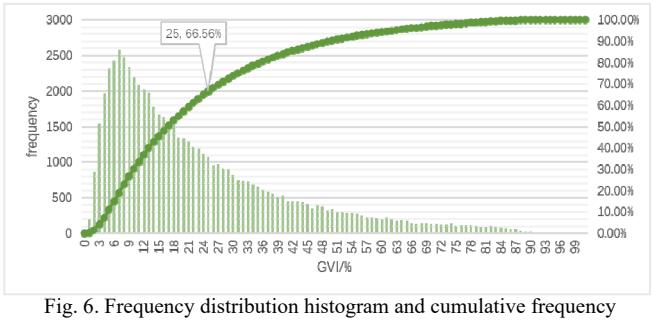

Fig. 6. Frequency distribution histogram and cumulative frequency distribution diagram.

5) GVI analysis by OSM road classification

According to the OpenStreetMap (OSM) road classification standards, the data covers 19 road types. Average GVI, standard deviation, variance, and median for different road types were calculated according to OSM standards. The following Fig. 7 illustrates the GVI for different road types:

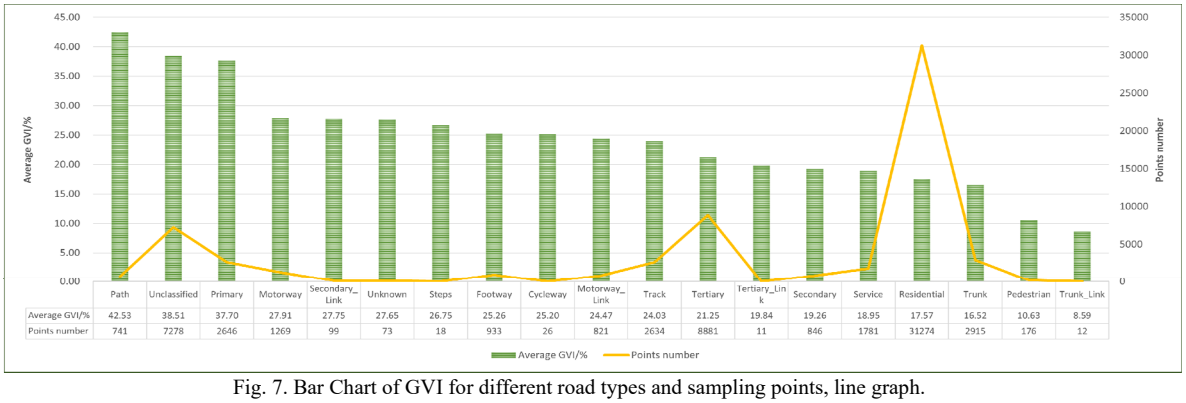

Fig. 7. Bar Chart of GVI for different road types and sampling points, line graph.

1) Significant differences exist between road types. The road type with the highest average GVI is ‘Path’, while the type with the lowest is ‘Trunk_Link’, with half of the road types having a GVI exceeding 25%.

2) Residential roads with the largest data volume show a lower average GVI of 17.57%. Additionally, sidewalks and service roads also have relatively low GVI values of 10.63% and 18.95%, respectively, significantly lowering

the overall city GVI level.

3) Generally, higher-level roads have higher GVI compared to lower-level roads.
4) Residential and central business district roads have universally lower GVI. Since these areas are hotspots for residential activity, low GVI may impact residents' travel experience, necessitating targeted optimization strategies for these areas.

6) GVI analysis by Japanese national road classification

In Japan, the OSM road classification standards are not entirely applicable. Therefore, OSM has provided annotations for Japanese road types [57]. According to Japanese road classification standards, there are 10 categories, as outlined and compared below:

Table 1. Comparison of Japanese road standards and OSM standards

Classification (JAPAN)	Classification (OSM)	Points	Points	Photos
Expressway	motorway	1269	2090	6270
	motorway_link	821		
National Highway	trunk	2915	2927	8781
	trunk_link	12		
Prefectural Road (Major)	primary	2646	2646	7938
Prefectural Road (General)	secondary	846	945	2835
	secondary_link	99		
General Road	tertiary	8881	16170	48510
	tertiary_link	11		
	unclassified	7278		
Residential Road	residential	31272	31272	93816
Community Road	service	1778	1778	5334
Pedestrian Path	pedestrian	176	1922	5766
	footway	931		
	path	740		
	steps	18		
	unknown	57		
Agricultural Road	track	2634	2634	7902
Bicycle Lane	cycleway	26	26	78
	SUM		62410	187230

High-level roads such as highways and national roads have high design speeds and good road conditions. Low-level roads include residential, service, pedestrian, bicycle, and forestry. As shown in Fig. 8, the analysis are as follows:

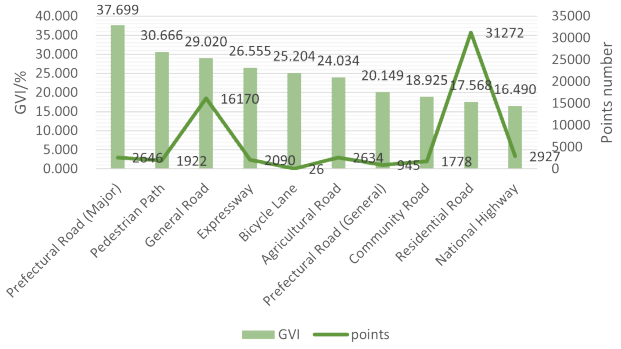

Fig. 8. Bar Chart of GVI for different road types and sampling points, line graph.

1) Residential roads have a GVI of 17.57%, and service roads, which are located in dense residential areas such as shopping malls and parking lots, have a GVI of 18.925%. Both road types are in residential areas and constitute a significant proportion of the total road length, directly affecting residents' urban travel experience and necessitating improvements in greening levels.
2) Higher-level roads generally meet the 25% GVI standard, whereas lower-level roads do not. This classification approach provides a clearer reflection of this characteristic compared to OSM road classifications.

Based on the comparison of the two classification systems, the following observations are made:

1) Low-level roads are often concentrated in residential and central business districts, which have relatively fewer large trees. Consequently, the GVI for these roads is lower compared to high-level roads.
2) Residential and commercial districts are characterized by a high density of buildings and high land utilization, resulting in less vegetation along roadsides and, thus, lower GVI.
3) High-level roads typically have fewer residential buildings along their sides, providing a wider view. Street view images from these roads capture the roadside greenery and distant green landscapes, leading to generally higher GVI.

7) GVI analysis by street view image capture time

The dataset includes the capture times of street view images. Due to climatic and seasonal factors, image capture is concentrated between April and September, accounting for over 90% of the data. This period covers spring, summer, and autumn in the Northern Hemisphere, when deciduous trees and shrubs are green. Therefore, the green proportion of streets during this time was relatively high, providing a better reflection of road GVI.

The vegetation condition along the roadsides directly influences the GVI. In Japan, a subtropical region, the greenness of roadside vegetation varies significantly across different seasons. Thus, a horizontal analysis of GVI by month is necessary. As shown in Fig. 9, the average GVI for different months was calculated, showing an increasing trend followed by a decrease, with the highest GVI observed in July, corresponding to peak vegetation growth. For January and February anomalous months, the low sample size (0.13%) and the higher GVI of data sources from specific road types contribute to the observed deviations.

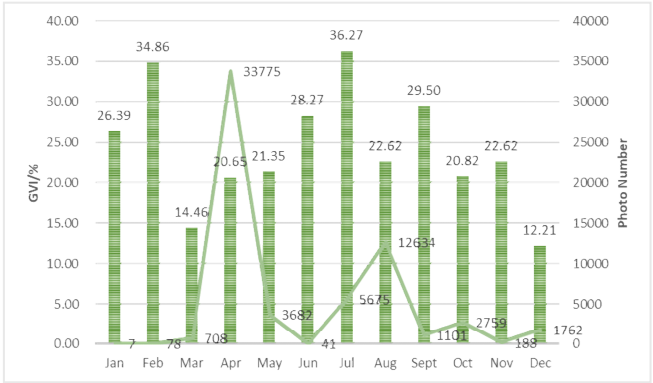

Fig. 9. Bar Chart of GVI for different months and sampling points line graph.

To minimize the impact of the growth cycles of deciduous trees and shrubs on GVI, the analysis focused on data from April to September. The average GVI for these six months is 22.87%, slightly higher than the annual average but not significantly different. As shown in Table 2, standard deviation, variance, and median also show minor increases.

Frequency distribution and cumulative frequency analysis reveal that the overall trend is consistent with previous analyses, with the peak frequency occurring at a GVI of 7%, slightly lower than previously observed. As shown in Fig. 10, the proportion of observation points with a GVI below 25% is 65.56%, showing a slight decrease.

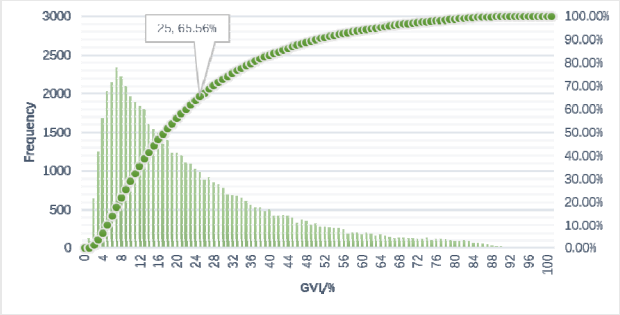

Fig. 10. Frequency distribution histogram and cumulative frequency distribution diagram.

Table 2. GVI statistics for different time periods

	Average value	Standard deviation	Variance	Median number
Half year	22.868	18.396	338.404	17.316
Whole year	22.397	18.292	334.586	16.826

C. Calculation and Analysis of NDVI

1) NDVI calculation

In ArcGIS 10.4, the NDVI values are computed using the raster calculator, employing the following formula:

$$NDVI = \frac{NIR - RED}{NIR + RED} \tag{3}$$

NIR and *RED* represent the reflectance in the near-infrared and red bands, respectively. NDVI values range from -1 to 1, with positive values indicating vegetation presence, and higher values denoting healthier and denser vegetation.

2) NDVI overall analysis

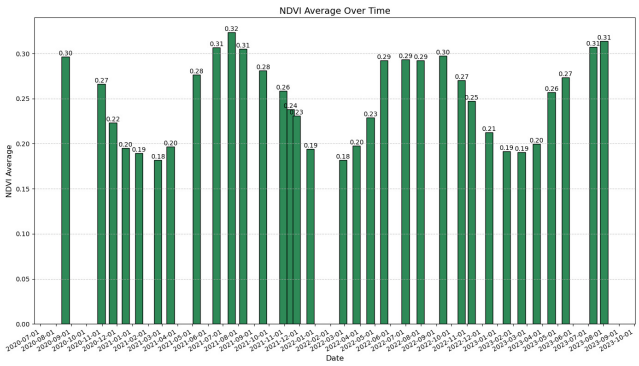

Fig. 11. NDVI trend from August 2020 to August 2023.

The overall NDVI trends were analyzed, and a general trend plot was created (as shown in Fig. 11). Based on 33 NDVI data sets, the mean NDVI value is 0.25 with a standard deviation of 0.17. Overall, NDVI values exhibit seasonal fluctuations, with peaks in summer (July and August) and troughs in winter (December and January). This trend is closely related to the plant growth cycle and climate conditions.

After analyzing the monthly NDVI averages (as shown in Fig. 12), it was found that May to September is the peak vegetation growth period values are at their highest. NDVI values gradually rise, peaking in July and August at around 0.31. NDVI values gradually decline, reaching a low of approximately 0.18 in January and February. This indicates that NDVI values in the study area exhibit pronounced seasonal characteristics.

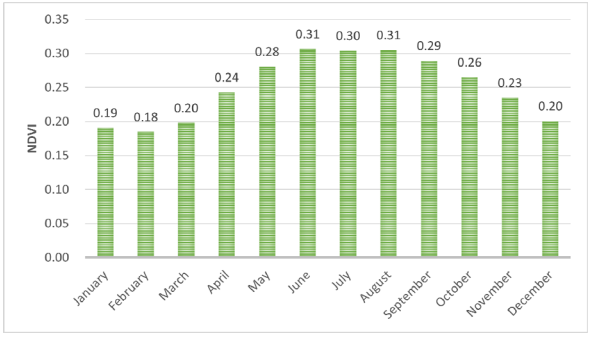

Fig. 12. Monthly NDVI average trend.

3) Curve fitting

Using Python to fit the monthly NDVI average values to functional curves, the following three fitting functions were obtained:

Table 3. Summary of fitting functions

Name	Formula	Mean Squared Error (MSE)
Trigonometric Functions	$0.06\times\sin(0.51\times x+4.08)+0.25$	0.00003890
Sine Function with Polynomial	$0.06\times\sin(0.53\times x+4.01)+0.00008\times x+0.25$	0.00003792
Cosine Function	$0.06\times\cos(0.51\times x+2.51)+0.25$	0.00003890

where sin() is the sine function and cos() is the cosine function.

The visual representation of the functions is shown in Fig. 13:

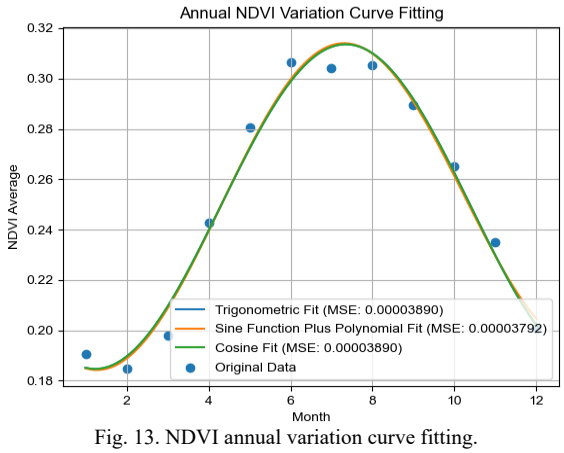

Fig. 13. NDVI annual variation curve fitting.

It was found that trigonometric functions provided the best fit because they can capture the periodic nature of the data, which aligns well with the seasonal periodicity of NDVI. By adjusting specific parameters such as amplitude, phase, and period, the function can be tailored to fit the data. of polynomial terms can also capture non-periodic fluctuations and trends, improving the fitting effect.

4) Correlation Analysis between GVI and NDVI

During the investigation, evidence indicated seasonal variations in GVI, mirrored the seasonal trends in NDVI.

This prompted an analysis of the correlation between GVI and NDVI, as it could provide further insights into GVI patterns. Monthly average values of GVI and NDVI were extracted for the analysis, as shown in the table below:

Table 4. Monthly comparison of GVI and NDVI

Month	Mean NDVI	Mean GVI
January	0.19063396	0.263929882
February	0.18462651	0.348648772
March	0.19798473	0.144624306
April	0.24288991	0.206500197
May	0.28073796	0.21352011
June	0.30654016	0.282730971
July	0.30418521	0.3627483
August	0.30515254	0.226247522
September	0.28936805	0.295042923
October	0.26497945	0.208229393
November	0.23484585	0.226154986
December	0.20062213	0.122148708

Due to noticeable errors in the GVI data for January and February, these two months were excluded from the analysis to ensure the reliability of the results. Since the GVI data for June and November is below 500, these two months are also considered for exclusion. Using Python's *Pearsonr(x, y)* function, the Pearson correlation coefficient between the average NDVI and GVI was calculated to be 0.83, indicating a strong positive correlation. As NDVI increases, GVI also tends to increase, and vice versa. As shown in Fig. 14, the scatter plot shows the relationship between the average NDVI and GVI, with a noticeable upward trend.

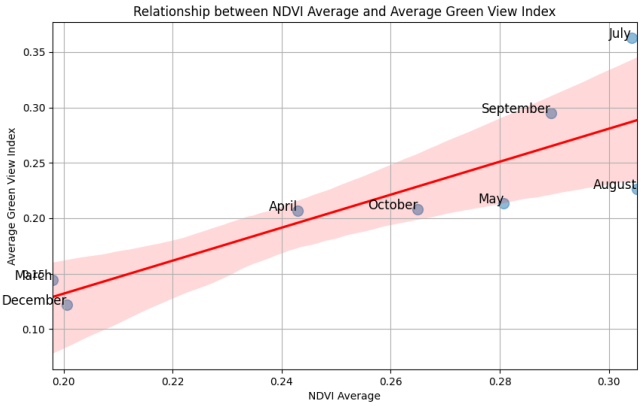

Fig. 14. Scatter plot.

Using Python's Ordinary Least Squares (OLS) regression analysis, the results indicated that NDVI has strong explanatory power for GVI (R^2 = 0.690), and the regression model is statistically significant (F-statistic = 13.37, p = 0.0106). The regression coefficient of NDVI is 1.4884, suggesting that for every unit increase in NDVI, GVI increases by approximately 1.4884 units. Diagnostic tests revealed that the residuals were approximately normally distributed, with no severe multicollinearity issues. Despite mild negative autocorrelation, the overall fit was satisfactory. The regression equation for average GVI is:

$$GVI = -0.1657 + 1.4884 \times NDVI \tag{4}$$

D. Calculation and Analysis of AQI

1) Calculation of AQI

Typically, the AQI is derived by calculating individual indices for various pollutants and adopting the most severe pollutant's value as the overall AQI. Different countries and regions employ distinct grading standards; for instance, Japan does not utilize the AQI but categorizes air quality into six distinct levels, each represented by a different color. For quantification and calculation, this study adopts the American AQI to substitute for Japan's color grading system [58].

The sub-index III for each pollutant can be computed using the following formula:

$$I = \frac{I_{high} - I_{low}}{C_{high} - C_{low}} \times (C - C_{\min}) + I_{low} \tag{5}$$

where I is sub-index of pollutants, C is concentration of the pollutant, C_{low} and C_{high} is lower and upper limits of concentration for the pollutant, C_{min} is lowest concentration of the pollutant, and I_{low} and I_{high} is lower and upper limits of corresponding pollutant index.

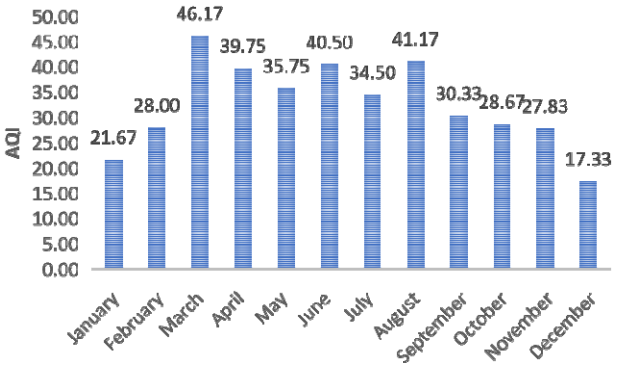

Fig. 15. Monthly AQI bar chart.

After calculating the sub-indices for each pollutant, it was determined that the AQI corresponding to PM2.5 is the highest. Consequently, PM2.5 was selected as the ultimate AQI. The foundational PM2.5 data and the monthly AQI data are presented in Fig. 15.

2) Analysis of AQI

The monthly AQI data for this study indicates that the overall air quality throughout the year is satisfactory, with an average AQI of 32.7. The highest recorded value is 46.2 in March, while the lowest is 17.3 in December. The air quality during most months falls within the excellent range, suggesting that air pollution in Hitachi City is relatively light, with no significant impact on public health.

Seasonally, air quality tends to be poorer in spring (March) and summer (June to August), with a slight increase in AQI levels, potentially attributable to seasonal dust storms, agricultural activities, and ozone pollution during the summer months. In contrast, the AQI steadily declines in autumn, with winter displaying the lowest values, particularly in December, when air quality peaks for the year. This improvement is likely due to meteorological conditions that favor the dispersion of air pollutants.

Overall, the air quality in Hitachi City demonstrates a favorable seasonal pattern, with urban greening and environmental management measures effectively maintaining high air quality levels for most of the year. However, attention must be directed toward potential pollution sources during the spring and summer to enhance air quality further.

E. Calculation and Analysis of LST

1) LST calculation

This study employs the Google Earth Engine platform to extract LST data from NASA's MODIS. Over three years, a total of 484 days of data were acquired. Given that this research operates on a monthly scale, the data for each month was averaged accordingly. The resulting data is presented in Fig. 16 below:

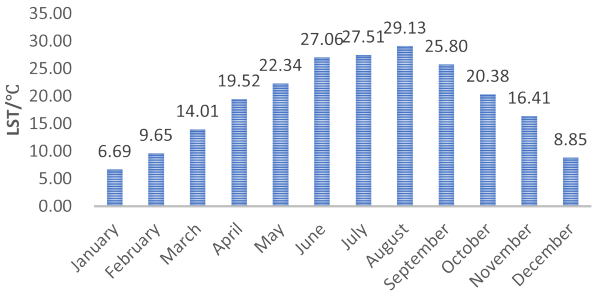

Fig. 16. Monthly LST bar chart.

2) LST analysis

The monthly LST data in this study reveal a pronounced seasonal variation throughout the year. The maximum temperature reaches 29.13°C in August, while the minimum dips to 6.69°C in January, indicating significant fluctuations in temperature with the changing seasons. During the winter and early spring months (January to March), temperatures are comparatively lower, with LST gradually rising month by month, reflecting the region's warming trend.

In the summer months (June to August), the LST peaks, with August recording the highest temperature of 29.13°C, marking it the hottest month of the year. This period is characterized by a pronounced urban heat island effect, which may lead to adverse environmental and health implications. In contrast, during autumn (September to November), the LST gradually declines, demonstrating the role of vegetation and urban greening in temperature regulation, particularly after October, when a notable decrease in surface temperature is observed.

Overall, the LST in Hitachi City exhibits significant seasonal variation, with urban greening playing a critical role in temperature moderation. Effective urban greening strategies, especially during the peak summer heat, can help mitigate the urban heat island effect and enhance the urban living environment.

F. Calculation and Analysis of Noise Pollution Data

1) Noise calculation

The traffic volumes at three entrances and exits of the Joban Expressway in Hitachi City have been statistically compiled monthly, differentiated by vehicle type. Given that traffic volume serves as a proxy, it is essential to convert these data into synchronized noise pollution metrics with Japan's prevailing automotive regulations. Under Japan's UN R51-03 regulation stipulations, various vehicle types are associated with distinct noise adjustment values [59]. This study systematically converts these values, yielding the following monthly aggregate noise levels as presented in Fig. 17 below:

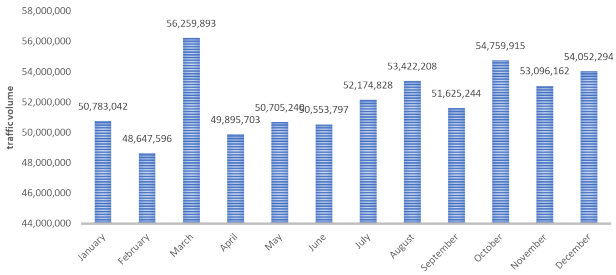

Fig. 17. Monthly noise bar chart.

2) Noise analysis

The analysis of monthly traffic volume and noise data from three highway entrances indicates that the noise index fluctuates throughout the year, reaching a peak of 56,259,893 in March and a trough of 48,647,596 in February. The correlation between noise data and traffic volume underscores the direct relationship between increased traffic flow and heightened noise pollution. The lowest noise index in February may be attributed to reduced traffic volumes due to holidays or meteorological conditions.

March and October represent the peak periods for noise indices, likely linked to seasonal increases in traffic flow or holiday travel surges. Notably, March recorded the highest noise index of the year, suggesting exceptionally high levels of traffic activity during this period, which exacerbates noise pollution and could adversely affect the quality of life for nearby residents.

Overall, the annual noise index remains relatively elevated, indicating significant noise pollution in areas with high traffic volumes, particularly during the summer and autumn months (June to October), when the noise index remains consistently high. This necessitates implementing soundproofing or traffic management measures to mitigate the negative impacts of noise on urban environments and public health.

G. Calculation of UGEQI

1) Outlier treatment

Due to the anomalous data in January, February, June, and November of the GVI, it is imperative to address these outliers before executing the UGEQI model calculations. The approach involves conducting a linear regression analysis utilizing the GVI and NDVI data from the remaining months to establish a regression model. Subsequently, this model is employed to derive the theoretical GVI values corresponding to the NDVI values from the four months. Finally, these theoretical GVI values are used to replace the outlier data, thereby ensuring the integrity and accuracy of the dataset. This method not only preserves the rationality of the data but also mitigates the potential influence of outliers on the final results.

2) Numerical standardization

All data must undergo 0-1 standardization to ensure comparability among different indicators. Standardization transforms raw data with varying dimensions—such as NDVI, AQI, and LST—into a uniform range, typically [0,1]. The standardization formula is as follows:

$$X' = \frac{X - X_{\min}}{X_{\max} - X_{\min}} \tag{6}$$

where X represents the original data, while X_{min} and X_{max} denote the minimum and maximum values of the indicator, respectively. X' signifies the standardized value. The following data is derived through the process of standardization:

Table 5. Summary of standardized data

Month	NDVI	GVI	LST	AQI	Noise Index
January	0.049	0.236	0.000	0.150	0.281
February	0.000	0.000	0.132	0.370	0.000
March	0.110	0.526	0.326	1.000	1.000
April	0.478	2.292	0.571	0.777	0.164
May	0.788	3.781	0.697	0.639	0.270
June	1.000	4.797	0.908	0.803	0.250
July	0.981	4.704	0.928	0.595	0.463
August	0.989	4.742	1.000	0.827	0.627
September	0.859	4.121	0.852	0.451	0.391
October	0.659	3.161	0.610	0.393	0.803
November	0.412	1.976	0.433	0.364	0.584
December	0.131	0.629	0.096	0.000	0.710

3) Model weight calculation

In this study, the model weights are calculated using the entropy method. Specifically, the first step involves determining the proportion of each indicator, which is obtained by dividing the value of a particular indicator in a given month by the total sum of that indicator over the twelve-month period. Subsequently, the entropy value for each indicator is computed using the following formula:

$$e_j = -\frac{1}{\ln(n)}\sum_{i=1}^{n} p_{ij}\ln(p_{ij}) \tag{7}$$

where e_j is entropy value of the j-th indicator, n is sample number (where is 12), and p_{ij} is the proportion of the j-th indicator in the i-th mouth.

Subsequently, the information utility value of each indicator is calculated using the entropy method, which is represented as $d_j = 1 - e_j$. Finally, the weights of each indicator are determined based on their respective information utility values, calculated as follows:

$$w_j = \frac{d_j}{\sum_{j=1}^{m} d_j} \tag{8}$$

where m is the number of indicators (which is 5).

The result is as follows:

Table 6. Weights of the UGEQI

NDVI	GVI	LST	AQI	Noise Index
0.247	0.246	0.192	0.145	0.169

The weight calculation results for the five UGEQI indicators reveal that the NDVI and the GVI each hold a weight of 0.246, representing the largest proportion. This finding underscores the significant impact of NDVI and GVI on environmental quality within urban greening initiatives, highlighting their pivotal roles in enhancing air quality, mitigating temperature fluctuations, and alleviating noise pollution. The dual effect of visual and vegetative elements is thus critical in elevating environmental quality.

The weight assigned to LST is 0.192, illustrating the importance of temperature regulation in the overall environmental quality, particularly during the summer months when elevated temperatures notably affect urban environments. Greening efforts play a proactive role in alleviating the urban heat island effect. Although the weight of LST is somewhat lower than that of NDVI and GVI, it remains a crucial factor influencing environmental quality, especially during periods of significant temperature variation.

The AQI and Noise Index weights are 0.145 and 0.169, respectively. This indicates that while air pollution and noise pollution negatively impact environmental quality, their roles within the UGEQI framework are relatively weaker. Nonetheless, considering their implications in urban life, they warrant attention, particularly in areas with high traffic flow and frequent industrial activities. These weights reflect the comprehensive influence of greening, temperature, air quality, and noise on urban environmental quality.

4) Analysis of UGEQI

Based on the weights derived from the entropy method, the calculation formula for the UGEQI is presented as follows:

$$UGEQI = 0.247\times GVI + 0.246\times NDVI + 0.145\times(1-AQI) + 0.192\times(1-LST) + 0.169\times(1-Noise\ Index) \tag{9}$$

As shown in Fig. 18, based on the provided UGEQI data, we observe trends in environmental quality variations across different months. Overall, the UGEQI values are highest in June and July, reaching 0.598 and 0.652, respectively, indicating relatively favorable environmental quality during these months. This may be attributed to the vigorous growth of vegetation and improved air quality in summer, reflecting the positive impact of urban greening on environmental quality during this season.

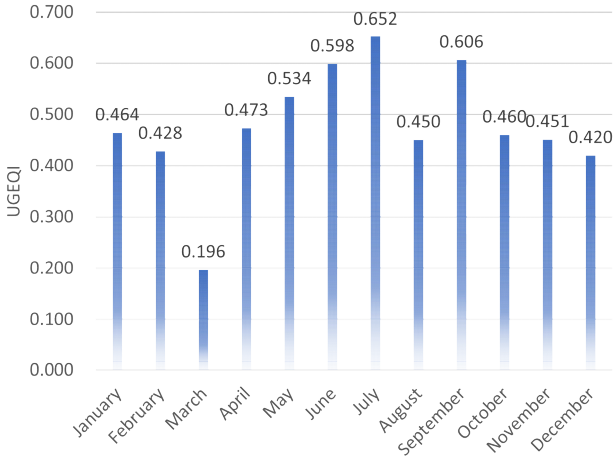

Fig. 18. Monthly UGEQI bar chart.

In contrast, the UGEQI value in March is the lowest, at only 0.196. This could be linked to seasonal climatic changes, the incomplete growth of vegetation, and increased pollutant concentrations. The low value in March indicates the challenges urban environmental quality faces during spring, particularly when vegetation has not yet been revived, which may negatively impact air quality and other environmental indicators.

Furthermore, although UGEQI values are relatively stable in most months, April, May, and September show higher environmental quality. This suggests that during the transitional seasons of late spring and early autumn, urban greening and climatic conditions work together to enhance

environmental quality. Therefore, it is recommended that urban greening efforts be strengthened in spring and summer to improve environmental quality and subsequently enhance residents' quality of life.

IV. Discussion

A. Assessment of Urban Greening Levels and Temporal-Spatial Variation Characteristics

This study elucidates the temporal and spatial distribution patterns of urban greening levels in Hitachi City by analyzing the GVI and the NDVI across different road types. The GVI along higher-grade roads is significantly greater than that along lower-grade roads, particularly in areas adjacent to highways and national roads. Seasonal variations in greening levels are also pronounced, with the highest greening observed in summer and a marked decline in winter, indicating that the temporal and spatial fluctuations of greening are closely related to the overall quality of the urban environment.

B. Effectiveness of the UGEQI Model and Comprehensive Assessment of Environmental Quality

The UGEQI model demonstrates that visual (GVI) and ecological (NDVI) greening are primary drivers of environmental quality (combined weight 49.3%), aligning with studies in Berkeley [26] and Shenzhen [60], where vegetation visibility and health reduced heat stress by 15-20%. Seasonal UGEQI peaks in summer (0.652) mirror findings in Raipur [61], where NDVI-LST correlations show a strong negative correlation. However, lower weights for AQI (14.5%) and noise (16.9%) contrast with Chile studies [33], where traffic noise dominated urban dissatisfaction. This discrepancy may stem from Hitachi's lower traffic density compared to megacities. Proxy noise data (traffic volume) also limits accuracy, echoing challenges in the USA [62]. Future work should integrate direct noise monitoring and long-term data to enhance robustness, as done in Singapore's 10-year green plan [63]

C. Practical Applications and Policy Recommendations

This research offers robust theoretical support for future urban planning and greening management in Hitachi City. The results indicate that areas with low GVI (such as residential and commercial zones) should prioritize increasing green space coverage and diversifying plant species in future planning to enhance environmental quality. Moreover, based on the UGEQI model, urban managers can adopt differentiated greening maintenance strategies across seasons; for example, intensifying green space maintenance in summer to further elevate environmental benefits and increasing the planting of evergreen species in winter to compensate for reduced vegetation cover.

D. Limitations

While the UGEQI model effectively assesses the impact of urban greening on environmental quality, certain limitations exist. Firstly, the proxy data for the noise index may not fully capture the noise pollution scenario. Future studies could incorporate more refined noise monitoring data to improve the accuracy of noise pollution assessments. Secondly, the relatively short time frame of the data prompts future research to explore long-term impacts of greening on environmental quality through more extensive temporal data acquisition. Lastly, although this study is based on Hitachi City, the differing socio-economic contexts in other cities may lead to variations in greening benefits; thus, cross-city comparative studies could validate the universality and applicability of the UGEQI model.

V. Conclusions

A. Multifaceted Impact of Greening on Urban Environmental Quality

The results indicate that urban greening significantly influences environmental quality across multiple dimensions. Primarily, visual greening (GVI) not only enhances the aesthetic experience for residents but also plays a crucial role in improving air quality, regulating temperature, and alleviating noise pollution. The strong correlation between GVI and NDVI further substantiates the close relationship between visual greening and the health of actual vegetation. This finding aligns with theories regarding the multifaceted improvements in environmental quality afforded by urban greening. However, further exploration of the complex interactions between GVI, air quality, and noise pollution is warranted for a more comprehensive understanding of the multidimensional benefits of greening.

B. Challenges and Potential of Multi-Source Data Fusion

Integrating diverse data sources (such as remote sensing data, street view images, and meteorological data) during data processing posed several challenges. Firstly, temporal and spatial resolution disparities among different data sources may result in biased assessments for specific periods or areas. Although data cleaning and standardization can mitigate this issue, future research should further investigate optimized methods for integrating multi-source data, especially regarding handling varying timeframes or missing data. Moreover, multi-source data fusion offers a more comprehensive and dynamic perspective for environmental quality assessment, particularly within urban planning and policy formulation.

C. Limitations of the UGEQI Model and Suggestions for Improvement

While the UGEQI model provides a comprehensive framework for evaluating urban environmental quality, certain shortcomings remain. Firstly, although the entropy method ensures the objectivity of indicator weight distribution, it fails to account for potential interactions among indicators, such as between GVI and LST, as well as NDVI and AQI. Future research could enhance model precision by incorporating multi-level models or considering coupling effects among indicators. Secondly, in this study, noise data served as a proxy based on traffic flow, which, while offering a rapid estimation method, may inadequately reflect actual noise pollution levels. Future analyses should utilize direct noise monitoring data or high-resolution noise maps for more detailed assessments.

D. In-Depth Exploration of Temporal-Spatial Characteristics in Urban Planning

This study reveals significant temporal-spatial

characteristics of urban greening, particularly concerning variations in GVI across different seasons and road types. These findings provide vital reference points for urban planners, indicating the need to consider road types and seasonal changes when optimizing greening layouts. For instance, in high-traffic roads and commercial areas, prioritizing planting tall trees and shrubs can enhance visual greening effects and mitigate traffic noise. Furthermore, maintaining greening in winter is a key area of focus; strategies to sustain greening effectiveness during colder months, thereby improving residents' quality of life, must not be overlooked in future greening plans.

E. Directions for Future Research

Certain assumptions and data processing methods in this study may influence the accuracy of the results. Future research could consider expanding the span of the survey to incorporate long-term data, facilitating an analysis of long-term trends in environmental quality. Additionally, future models may integrate socio-economic data (such as population density and changes in traffic flow) to comprehensively assess the combined impact of urban greening on residents' quality of life. Cross-city comparative studies exploring the disparities in greening effects across different urban contexts will further validate the applicability of the UGEQI model in broader scenarios.

Conflict of Interest

The authors declare no conflict of interest.

Author Contributions

Dongmin Yin conducted the research, analyzed data, and drafted the manuscript. Terumitsu Hirata supervised the study, provided critical guidance on methodology and interpretation, and contributed to the manuscript's review and final approval; all authors had approved the final version.

References

[1] S. Wang, S. Gao, S. Li, and K. Feng, "Strategizing the relation between urbanization and air pollution: Empirical evidence from global countries," *J. Clean. Prod.*, vol. 243, 118615, Jan. 2020. doi: 10.1016/j.jclepro.2019.118615.

[2] J. M. B. Morillas, G. R. Gozalo, D. M. González, P. A. Moraga, and R. Vílchez-Gómez, "Noise Pollution and Urban Planning," *Curr. Pollut. Rep.*, vol. 4, no. 3, pp. 208–219, Sep. 2018. doi: 10.1007/s40726-018-0095-7.

[3] A. Piracha and M. T. Chaudhary, "Urban air pollution, urban heat island and human health: A review of the literature," *Sustainability*, vol. 14, no. 15, 9234, Jul. 2022. doi: 10.3390/su14159234.

[4] E. Piano *et al.*, "Urbanization drives cross-taxon declines in abundance and diversity at multiple spatial scales," *Glob. Change Biol.*, vol. 26, no. 3, pp. 1196–1211, Mar. 2020. doi: 10.1111/gcb.14934.

[5] S. Hankey and J. D. Marshall, "Urban form, air pollution, and health," *Curr. Environ. Health Rep.*, vol. 4, no. 4, pp. 491–503, Dec. 2017. doi: 10.1007/s40572-017-0167-7.

[6] P. Li and Z.-H. Wang, "Environmental co-benefits of urban greening for mitigating heat and carbon emissions," *J. Environ. Manage.*, vol. 293, 112963, Sep. 2021. doi: 10.1016/j.jenvman.2021.112963.

[7] E. Quaranta, C. Dorati, and A. Pistocchi, "Water, energy and climate benefits of urban greening throughout Europe under different climatic scenarios," *Sci. Rep.*, vol. 11, no. 1, 12163, Jun. 2021. doi: 10.1038/s41598-021-88141-7.

[8] N. Tomson, R. N. Michael, and I. E. Agranovski, "Removal of particulate air pollutants by Australian vegetation potentially used for green barriers," *Atmospheric Pollut. Res.*, vol. 12, no. 6, 101070, Jun. 2021. doi: 10.1016/j.apr.2021.101070.

[9] W. Yang, Z. Wang, P. Hua, J. Zhang, and P. Krebs, "Impact of green infrastructure on the mitigation of road-deposited sediment induced stormwater pollution," *Sci. Total Environ.*, vol. 770, 145294, May 2021. doi: 10.1016/j.scitotenv.2021.145294.

[10] P. P. Joshi *et al.*, *An Ecological Framework for Greening Cities*, 2016.

[11] L. Mata *et al.*, "Large ecological benefits of small urban greening actions," Jul. 25, 2021. doi: 10.1101/2021.07.23.453468.

[12] A. Dzhambov and D. Dimitrova, "Urban green spaces' effectiveness as a psychological buffer for the negative health impact of noise pollution: A systematic review," *Noise Health*, vol. 16, no. 70, p. 157, 2014. doi: 10.4103/1463-1741.134916.

[13] M. F. Jonker, F. J. Van Lenthe, B. Donkers, J. P. Mackenbach, and A. Burdorf, "The effect of urban green on small-area (healthy) life expectancy," *J. Epidemiol. Community Health*, vol. 68, no. 10, pp. 999–1002, Oct. 2014. doi: 10.1136/jech-2014-203847.

[14] B. Ma, T. Zhou, S. Lei, Y. Wen, and T. T. Htun, "Effects of urban green spaces on residents' well-being," *Environ. Dev. Sustain.*, vol. 21, no. 6, pp. 2793–2809, Dec. 2019. doi: 10.1007/s10668-018-0161-8.

[15] L. Yuan, K. Shin, and S. Managi, "Subjective well-being and environmental quality: The impact of air pollution and green coverage in China," *Ecol. Econ.*, 2018. doi: 10.1016/J.ECOLECON.2018.04.033.

[16] M. Kondo, J. Fluehr, T. McKeon, and C. Branas, "Urban green space and its impact on human health," *Int. J. Environ. Res. Public. Health*, vol. 15, no. 3, p. 445, Mar. 2018. doi: 10.3390/ijerph15030445.

[17] J. Maas, P. Spreeuwenberg, M. Van Winsum-Westra, R. A. Verheij, S. Vries, and P. P. Groenewegen, "Is green space in the living environment associated with people's feelings of social safety?" *Environ. Plan. Econ. Space*, vol. 41, no. 7, pp. 1763–1777, Jul. 2009. doi: 10.1068/a4196.

[18] S. Bonilla-Bedoya, A. Estrella, F. Santos, and M. Á. Herrera, "Forests and urban green areas as tools to address the challenges of sustainability in Latin American urban socio-ecological systems," *Appl. Geogr.*, vol. 125, p. 102343, Dec. 2020. doi: 10.1016/j.apgeog.2020.102343.

[19] A. D. L. I. Martinez and S. M. Labib, "Demystifying Normalized Difference Vegetation Index (NDVI) for greenness exposure assessments and policy interventions in urban greening," *SSRN Electron. J.*, 2022. doi: 10.2139/ssrn.4207665.

[20] W. Lin *et al.*, "The effect of green space behaviour and per capita area in small urban green spaces on psychophysiological responses," *Landsc. Urban Plan.*, vol. 192, 103637, Dec. 2019. doi: 10.1016/j.landurbplan.2019.103637.

[21] B. L. Ong, "Green plot ratio: An ecological measure for architecture and urban planning," *Landsc. Urban Plan.*, vol. 63, no. 4, pp. 197–211, May 2003. doi: 10.1016/S0169-2046(02)00191-3.

[22] J. Ma, X. Yan, W. Dong, and J. Chou, "Gross primary production of global forest ecosystems has been overestimated," *Sci. Rep.*, vol. 5, no. 1, 10820, Jun. 2015. doi: 10.1038/srep10820.

[23] Y. Tian and G. Fu, "Quantifying plant species α-diversity using normalized difference vegetation index and climate data in alpine grasslands," *Remote Sens.*, vol. 14, no. 19, p. 5007, Oct. 2022. doi: 10.3390/rs14195007.

[24] A. Toikka, E. Willberg, V. Mäkinen, T. Toivonen, and J. Oksanen, "The green view dataset for the capital of Finland, Helsinki," *Data Brief*, vol. 30, 105601, Jun. 2020. doi: 10.1016/j.dib.2020.105601.

[25] R. Dong, Y. Zhang, and J. Zhao, "How green are the streets within the sixth ring road of Beijing? An analysis based on tencent street view pictures and the green view index," *Int. J. Environ. Res. Public. Health*, vol. 15, no. 7, p. 1367, Jun. 2018. doi: 10.3390/ijerph15071367.

[26] J. Yang, L. Zhao, J. Mcbride, and P. Gong, "Can you see green? Assessing the visibility of urban forests in cities," *Landsc. Urban Plan.*, vol. 91, no. 2, pp. 97–104, Jun. 2009. doi: 10.1016/j.landurbplan.2008.12.004.

[27] L. Su, W. Chen, Y. Zhou, L. Fan, and J. Li, "Exploring urban street green perception from the perspective of combining GVI and NDVI: A Case study of Zhongshan City, Guangdong Province," BioRxiv, May 23, 2023. doi: 10.1101/2023.05.21.541659.

[28] A. Monteiro, M. Vieira, C. Gama, and A. I. Miranda, "Towards an improved air quality index," *Air Qual. Atmosphere Health*, vol. 10, no. 4, pp. 447–455, May 2017. doi: 10.1007/s11869-016-0435-y.

[29] D. Long *et al.*, "Generation of MODIS-like land surface temperatures under all-weather conditions based on a data fusion approach," *Remote Sens. Environ.*, vol. 246, 111863, Sep. 2020. doi: 10.1016/j.rse.2020.111863.

[30] R. Wang *et al.*, "Residential greenness, air pollution and psychological well-being among urban residents in Guangzhou, China," *Sci. Total Environ.*, vol. 711, 134843, Apr. 2020. doi: 10.1016/j.scitotenv.2019.134843.

[31] R. Wang *et al.*, "Urban greenery and mental wellbeing in adults: Cross-sectional mediation analyses on multiple pathways across different greenery measures," *Environ. Res.*, vol. 176, 108535, Sep. 2019. doi: 10.1016/j.envres.2019.108535.

[32] K. R. Gunawardena, M. J. Wells, and T. Kershaw, "Utilising green and

bluespace to mitigate urban heat island intensity," *Sci. Total Environ.*, vol. 584–585, pp. 1040–1055, Apr. 2017. doi: 10.1016/j.scitotenv.2017.01.158.
[33] G. Rey Gozalo, E. Suárez, A. L. Montenegro, J. P. Arenas, J. M. Barrigón Morillas, and D. Montes González, "Noise estimation using road and urban features," *Sustainability*, vol. 12, no. 21, p. 9217, Nov. 2020. doi: 10.3390/su12219217.
[34] Y. Lu, "Using Google Street View to investigate the association between street greenery and physical activity," *Landsc. Urban Plan.*, vol. 191, p. 103435, Nov. 2019. doi: 10.1016/j.landurbplan.2018.08.029.
[35] L. Zhang, P. Y. Tan, and D. Richards, "Relative importance of quantitative and qualitative aspects of urban green spaces in promoting health," *Landsc. Urban Plan.*, vol. 213, 104131, Sep. 2021. doi: 10.1016/j.landurbplan.2021.104131.
[36] R. Wang, Y. Lu, X. Wu, Y. Liu, and Y. Yao, "Relationship between eye-level greenness and cycling frequency around metro stations in Shenzhen, China: A big data approach," *Sustain. Cities Soc.*, vol. 59, p. 102201, Aug. 2020. doi: 10.1016/j.scs.2020.102201.
[37] Y. Sun *et al.*, "Using machine learning to examine street green space types at a high spatial resolution: Application in Los Angeles County on socioeconomic disparities in exposure," *Sci. Total Environ.*, vol. 787, 147653, Sep. 2021. doi: 10.1016/j.scitotenv.2021.147653.
[38] Y. Zhang, S. Li, X. Fu, and R. Dong, "Quantification of urban greenery using hemisphere-view panoramas with a green cover index," *Ecosyst. Health Sustain.*, vol. 7, no. 1, 1929502, Jan. 2021. doi: 10.1080/20964129.2021.1929502.
[39] T. Aikoh, R. Homma, and Y. Abe, "Comparing conventional manual measurement of the green view index with modern automatic methods using google street view and semantic segmentation," *Urban For. Urban Green.*, vol. 80, 127845, Feb. 2023. doi: 10.1016/j.ufug.2023.127845.
[40] T. Kameoka, A. Uchida, Y. Sasaki, and T. Ise, "Assessing streetscape greenery with deep neural network using Google Street View," *Breed. Sci.*, vol. 72, no. 1, pp. 107–114, 2022. doi: 10.1270/jsbbs.21073.
[41] X. Yu, G. Zhao, C. Chang, X. Yuan, and F. Heng, "BGVI: A new index to estimate street-side greenery using baidu street view image," *Forests*, vol. 10, no. 1, p. 3, Dec. 2018. doi: 10.3390/f10010003.
[42] L. Cheng, S. Chu, W. Zong, S. Li, J. Wu, and M. Li, "Use of tencent street view imagery for visual perception of streets," *ISPRS Int. J. Geo-Inf.*, vol. 6, no. 9, p. 265, Aug. 2017. doi: 10.3390/ijgi6090265.
[43] ESA-Sentinel-2. (Aug. 10, 2024). [Online]. Available: https://www.esa.int/Applications/Observing_the_Earth/Copernicus/Sentinel-2
[44] Ibaraki Prefecture. Ibaraki's Environment (List of Measurement Results). Ibaraki Prefecture [In Japanese]. (Oct. 18, 2024). [Online]. Available: https://www.pref.ibaraki.jp/seikatsukankyo/kantai/data/index.html
[45] C. Yang *et al.*, "The effect of urban green spaces on the urban thermal environment and its seasonal variations," *Forests*, vol. 8, no. 5, p. 153, May 2017. doi: 10.3390/f8050153.
[46] Google Earth Engine. (Oct. 17, 2024). [Online]. Available: https://earthengine.google.com
[47] Ministry of the Environment. Status of Automobile Traffic Noise. (Oct. 16, 2024). [Online]. Available: https://www.env.go.jp/air/car/noise/index.html
[48] Hitachi City Official Website. Hitachi City Statistics: 7 Transportation and Communications | Hitachi City Official Website. (Oct. 16, 2024). [Online]. Available: https://www.city.hitachi.lg.jp/opendata/datalist/1003588/1003603.html
[49] J. Zhang and A. Hu, "Analyzing green view index and green view index best path using Google street view and deep learning," *J. Comput. Des. Eng.*, vol. 9, no. 5, pp. 2010–2023, Oct. 2022. doi: 10.1093/jcde/qwac102.
[50] V. Badrinarayanan, A. Kendall, and R. Cipolla, "SegNet: A deep convolutional encoder-decoder architecture for image segmentation," *IEEE Trans. Pattern Anal. Mach. Intell.*, vol. 39, no. 12, pp. 2481–2495, Dec. 2017. doi: 10.1109/TPAMI.2016.2644615.
[51] G. Fu, C. Liu, R. Zhou, T. Sun, and Q. Zhang, "Classification for high resolution remote sensing imagery using a fully convolutional network," *Remote Sens.*, vol. 9, no. 5, p. 498, May 2017. doi: 10.3390/rs9050498.
[52] F.-C. Chen, "Back-propagation neural networks for nonlinear self-tuning adaptive control," *IEEE Control Syst. Mag.*, vol. 10, no. 3, pp. 44–48, Apr. 1990. doi: 10.1109/37.55123.
[53] L.-C. Chen, G. Papandreou, I. Kokkinos, K. Murphy, and A. L. Yuille, "DeepLab: Semantic image segmentation with deep convolutional nets, Atrous convolution, and fully connected cRFs," *IEEE Trans. Pattern Anal. Mach. Intell.*, vol. 40, no. 4, pp. 834–848, Apr. 2018. doi: 10.1109/TPAMI.2017.2699184.
[54] Recent Research | Urban Research Department Urban Development Research Lab. (Aug. 10, 2024). [Online]. Available: https://www.nilim.go.jp/lab/jeg/current-fields.html
[55] Social experiment survey on the correlation between the amount of greenery in cities and psychological effects - The landscape and psychological effects of greenery in cities in mitigating discomfort on midsummer days. (Aug. 10, 2024). [Online]. Available: https://www.mlit.go.jp/kisha/kisha05/04/040812_3_.html
[56] Kyoto City: Kyoto City Green Master Plan" [2010-2025]," Kyoto City Information Center. (Aug. 06, 2024). [Online]. Available: https://www.city.kyoto.lg.jp/kensetu/page/0000077122.html
[57] JA:Japan tagging - OpenStreetMap Wiki. (Jul. 09, 2024). [Online]. Available: https://wiki.openstreetmap.org/wiki/JA:Japan_tagging#%E9%81%93%E8%B7%AF%E3%81%AE%E7%A8%AE%E5%88%A5
[58] Air Quality Index - Wikipedia. (Oct. 18, 2024). [Online]. Available: https://ja.wikipedia.org/wiki/%E7%A9%BA%E6%B0%97%E8%B3%AA%E6%8C%87%E6%95%B0#cite_note-sor-g5-20
[59] Automobiles: Environmental Measures-Ministry of Land, Infrastructure, Transport and Tourism. (Oct. 17, 2024). [Online]. Available: https://www.mlit.go.jp/jidosha/kankyo.html
[60] X. Jing, Z. Li, H. Chen, and C. Zhang, "'Is what we see always real?' A Comparative study of two-dimensional and three-dimensional Urban green spaces: The case of Shenzhen's central district," *Forests*, vol. 15, no. 6, p. 983, Jun. 2024. doi: 10.3390/f15060983.
[61] S. Guha and H. Govil, "Seasonal variability of LST-NDVI correlation on different land use/land cover using Landsat satellite sensor: A case study of Raipur City, India," *Environ. Dev. Sustain.*, vol. 24, no. 6, pp. 8823–8839, Jun. 2022. doi: 10.1007/s10668-021-01811-4.
[62] M. R. Cook, K. L. Gee, Mark. K. Transtrum, and S. V. Lympany, "Toward a dynamic national transportation noise map: Modeling temporal variability of traffic volume," *J. Acoust. Soc. Am.*, vol. 154, no. 5, pp. 2950–2958, Nov. 2023. doi: 10.1121/10.0022356.
[63] Singapore Green Plan 2030. (Mar. 29, 2025). [Online]. Available: https://www.greenplan.gov.sg/